# A Novel Method for Fabricating Chemically Defined Patterns as Standard Samples for Surface Chemical Imaging

Miki Akiyama, Mitsuhiro Fujita, and Masamichi Fujihira*
*Department of Biomolecular Engineering, Tokyo Institute of Technology, 4259 Nagatsuta, Midori-ku, Yokohama 226-8501*

(Received July 10, 2006; CL-060774; E-mail: mfujihir@bio.titech.ac.jp)

To produce micrometer scale chemical patterns, a new method is developed. In this method, silica beads are used as a mask of an underneath substrate. We produced the patterns with $CH_3$- and COOH-terminated regions and compared them with similar patterns prepared by the microcontact printing ($\mu$CP) method. The advantage of this technique over $\mu$CP is that monolayers with higher chemical purity can be patterned: thus it provides ideal and well-defined standard samples for surface chemical imaging such as chemical force microscopy.

Mapping of surface forces such as friction force[1] and adhesive force using scanning probe microscopy (SPM) has been used for imaging lateral distribution of outermost surface chemical properties. Chemical imaging by SPM with molecularly modified probe tips[2] is called chemical force microscopy (CFM).[3] In order to understand the chemical contrast of CFM, extensive studies have been conducted on surface chemical interaction at molecular level using SPM.[4–9] In such studies, chemically patterned surfaces have been frequently used to avoid fluctuation caused by experimental factors such as shape and coating of the tip apex.[10,11] One of the representative patterning techniques is microcontact printing ($\mu$CP).[12] However, the chemical patterns prepared by $\mu$CP have some limitation, i.e., the monolayers printed by $\mu$CP are not chemically pure because of insufficient ink transfer.[13,14] Therefore, careful attention should be paid to the defects in the monolayer patterned by $\mu$CP.

In this letter, we describe a new method where silica beads are used to make patterns. Two constituent parts of the patterns are both formed in solution, and hence defects must be few. The patterned surfaces prepared by the present method are compared with those by $\mu$CP using atomic force microscopy (AFM) and friction force microscopy (FFM).

Figure 1 shows a schematic diagram of the fabrication process of chemically patterned surfaces using silica beads. Gold films were deposited on cleaned cover glass plates with a Hitachi E-1030 ion sputter coater using argon plasma at ca. 6 Pa and 15 mA with a deposition rate of about 11 nm min$^{-1}$ for 90 s. First, the substrate was reacted with a 1 mM $CH_3(CH_2)_{19}SH$ ethanol solution for 15 min (Figure 1a). Second, a drop of the dilute ethanol suspension of silica beads (0.1 wt %) was placed on the gold surface. The beads were purchased from Lancaster and the nominal diameter was 0.5 μm. However, the diameter was determined to be 0.45 μm from AFM images (not shown here). The substrate was allowed to stand until all of the ethanol was evaporated (Figure 1b). After this, gold was again sputter-coated on the bead-covered plate for 20 s with the same deposition rate (Figure 1c). The substrate was then further reacted with a 1 mM $HOOC(CH_2)_{10}SH$ ethanol solution for 15 min (Figure 1d). Finally, the silica beads were removed in ethanol by ultrasonication (Figure 1e). The process was repeated in reverse order, beginning with deposition of $HOOC(CH_2)_{10}SH$.

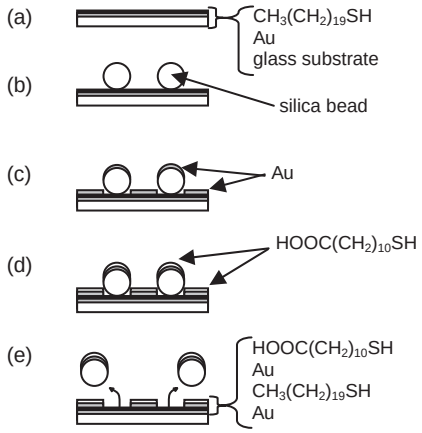


**Figure 1.** A preparation procedure of patterned samples using silica beads.

A patterned surface by $\mu$CP was prepared using the wet-inking method as described previously.[11] The 1 mM ethanol solution of $CH_3(CH_2)_{19}SH$ was used as the inking solution and the time of contact was 15 s. The patterned surface was further reacted with a 1 mM $HOOC(CH_2)_{10}SH$ ethanol solution for 15 min.

All AFM and FFM measurements were performed using a commercial AFM (a SEIKO Instruments SPA400 AFM unit with an SPI3800N AFM controller) and a rectangular cantilever with a $Si_3N_4$ pyramidal tip (Olympus RC800PSA-1 with a spring constant of 0.12 N m$^{-1}$). In addition to the topographic images (AFM images), the frictional images (FFM images) in both trace and retrace directions were captured. The scan rate for AFM and FFM was 1 Hz, and the cantilever bending force[15] for AFM and FFM was ca. 10 nN. Frictional data were recorded as photodiode output in volts. Then, the subtraction of friction data at each point of the trace and retrace frictional images, which is referred to as friction force signals, was calculated and the histogram of the friction force signals was created. All the measurements were performed under ambient condition.

Figures 2a and 2b show a topographic and a friction force image, respectively, of surface prepared by the process shown in Figure 1. In Figure 2a, the darker parts correspond to lower heights. The circular shape of craters was obviously formed by removal of beads. The size of the craters is slightly smaller than the size of beads because gold particles spread a little under beads owing to the presence of gold sputtered with the incident angles other than the normal incidence. However, we conclude its effect is not significant because the images show well-defined contrast both in a topographic and a friction force image. The

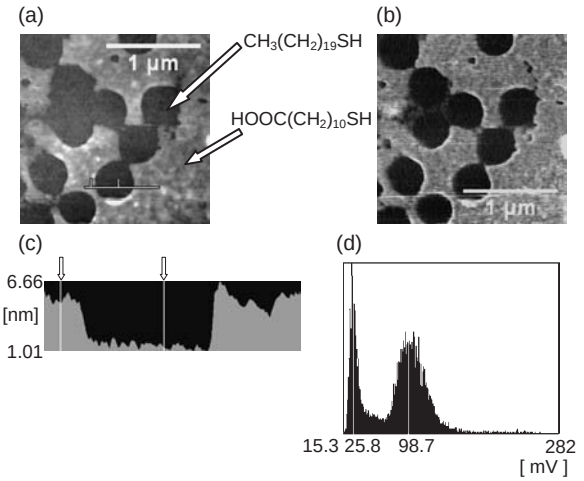


**Figure 2.** (a) A $2 \times 2\,\mu m^2$ topographic (range from 0.98 to 6.68 nm) and (b) a friction force image of the pattern prepared by the silica beads method illustrated in Figure 1. (c) Cross section of the topographic image along a solid line in Figure 2a. Steps of ca. 4 nm indicated by white arrows correspond to the difference in height between the $CH_3$- and COOH-terminated regions. (d) A friction force histogram from data in Figure 2b and its retrace image (not shown here).

height differences between the two regions are ca. 4 nm (Figure 2c), which well agree to the thickness of sputter-coated gold for 20 s shown in Figure 1c. In Figure 2b, the brighter parts correspond to higher friction force regions. The COOH-terminated regions outside the circle show higher friction than the $CH_3$-terminated regions inside the circle. This is because the COOH-terminated regions have the higher coefficient of friction due to the higher adhesion of the polar surface to the $Si_3N_4$ tip.[15,16] Figure 2d shows a histogram of the friction force signals from data in Figure 2b and its retrace friction force image (not shown in Figure 2). In this histogram, averaged friction force signals on the $CH_3$- and COOH-terminated regions were found to be 25.8 and 98.7 mV, respectively. These two peaks are broadened because of the roughness of the sputtered gold.[17] The COOH-terminated regions showed 3.83 times higher friction than the $CH_3$-terminated regions.

Figures 3a and 3b show a topographic and a friction force image, respectively, of a sample, in which the $CH_3$- and COOH-terminated regions are reversed from Figure 2 (i.e., the inside of the circle is the COOH-terminated, and the surrounding is the $CH_3$-terminated regions). Compared with Figures 2a and 2b, the topographic image shows a similar contrast, while the friction force image shows the reversed contrast. From the histogram (not shown) of friction force from data in Figure 3b and its retrace image, averaged friction force signals on the $CH_3$- and COOH-terminated regions were found to be 34.7 and 134.1 mV, respectively. The COOH-terminated regions showed 3.86 times higher friction than the $CH_3$-terminated regions. It should be noted that the friction force signals observed in Figures 2 and 3 cannot be compared directly because the sensitivity of the friction force signals to actual friction force was changed when the optical axis was retuned after the sample exchange.

Little difference (only 1%) was observed in the frictional ratios between the two samples, indicating that the effect of difference in the gold thickness (i.e., difference in the surface roughness) seems to be little compared with the effect of difference in the terminal groups. Therefore, the contrast in friction reflects the chemical composition of the monolayers.

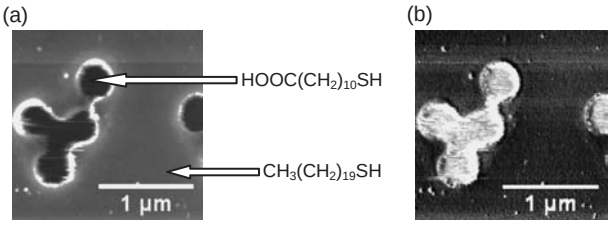


**Figure 3.** (a) A $2 \times 2\,\mu m^2$ topographic (range from 0 to 29.5 nm) and (b) a friction force image of a pattern prepared in the reverse order. The FFM contrast of Figure 3b between $CH_3$- and COOH-terminated regions is reversed from that in Figure 2b.

In addition, a histogram was also created from friction force data captured on a $\mu$CP sample, and averaged friction force signals on the $CH_3$- and COOH-terminated regions were found to be 26.1 and 61.7 mV, respectively (not shown). The COOH-terminated regions showed 2.36 times higher friction than the $CH_3$-terminated regions. We supposed that mixed monolayers were formed over the printed area through further chemisorption of $HOOC(CH_2)_{10}SH$ during the second reaction in its ethanol solution because of the high defect concentration in the printed area.[13,14] As a result, the printed $CH_3$-terminated area became more polar and the contrast became lower.

In conclusion, the observed contrast in friction on chemical patterns prepared by the silica beads method was much higher than that by $\mu$CP, i.e., the monolayers prepared by the present method had higher chemical purity than those by $\mu$CP, indicating that the new method provides ideal standard samples for surface chemical imaging such as CFM.

**References**

1 R. M. Overney, E. Meyer, J. Frommer, D. Brodbeck, R. Luthi, L. Howald, H.-J. Guntherodt, M. Fujihira, H. Takano, Y. Gotoh, *Nature* **1992**, *359*, 133.
2 T. Nakagawa, K. Ogawa, T. Kurumizawa, S. Ozaki, *Jpn. J. Appl. Phys.* **1993**, *32*, L294.
3 C. D. Frisbie, L. F. Rozsnyai, A. Noy, M. S. Wrighton, C. M. Lieber, *Science* **1994**, *265*, 2071.
4 H. Schonherr, C. L. Feng, N. Tomczak, G. J. Vancso, *Macromol. Symp.* **2005**, *230*, 149.
5 A. Takahara, Y. Hara, K. Kojio, T. Kajiyama, *Collloids. Surf. B* **2002**, *23*, 141.
6 T. Koga, H. Otsuka, A. Takahara, *Bull. Chem. Soc. Jpn.* **2005**, *78*, 1691.
7 K. Iimura, T. Shiraku, T. Kato, *Langmuir* **2002**, *18*, 10183.
8 R. W. Carpick, M. Salmeron, *Chem. Rev.* **1997**, *97*, 1163.
9 S. Lee, A. Puck, M. Graupe, R. Colorado, Y.-S. Shon, T. R. Lee, S. S. Perry, *Langmuir* **2001**, *17*, 7364.
10 J. E. Houston, C. M. Doelling, T. K. Vanderlick, Y. Hu, G. Scoles, I. Wenzl, T. R. Lee, *Langmuir* **2005**, *21*, 3926.
11 M. Fujihira, M. Furugori, U. Akiba, Y. Tani, *Ultramicroscopy* **2001**, *86*, 75.
12 A. Kumar, G. M. Whitesides, *Appl. Phys. Lett.* **1993**, *63*, 2002.
13 N. B. Larsen, H. Biebuyck, E. Delamarche, B. Michel, *J. Am. Chem. Soc.* **1997**, *119*, 3017.
14 F. Sato, H. Okui, K. Akimoto, M. Fujihira, *PMSE Preprints* **2004**, *90*, 144.
15 M. Fujihira, D. Aoki, Y. Okabe, H. Takano, H. Hokari, J. Frommer, Y. Nagatani, F. Sakai, *Chem. Lett.* **1996**, 499.
16 N. J. Brewer, B. D. Beake, G. J. Leggett, *Langmuir* **2001**, *17*, 1970.
17 F. Sato, H. Okui, U. Akiba, K. Suga, M. Fujihira, *Ultramicroscopy* **2003**, *97*, 303.

Published on the web (Advance View) September 2, 2006; doi:10.1246/cl.2006.1112